Geomechanics and Engineering, *Vol. 42, No. 1 (2025) 15-29*
https://doi.org/10.12989/gae.2025.42.1.015

Prediction of drawdown and retaining structure deformation under the influence of foundation pit dewatering and excavation based on unsteady seepage

Kunpeng Li[1a], Shihai Chen*[1], Weiyu Chen[2b] and Gangnan Ye[3c]

[1]*College of Civil Engineering, Huaqiao University, Xiamen, Fujian, China*
[2]*Fujian Yongwang Construction Group Co., Ltd, Longyan, Fujian, China*
[3]*Fujian Mingtai Group Co., Ltd, Xiamen, Fujian, China*

(*Received November 23, 2024, Revised June 23, 2025, Accepted June 24, 2025*)

Abstract. Existing theories for calculating the horizontal displacement of retaining structures do not simultaneously consider the effects of dewatering and excavation. The dewatering leads to drawdown and the seepage force, the excavation leads to the change of soil pressure. Under the combined effects of both factors, the distribution of water and soil pressure on both sides of the retaining structure is reassigned, resulting in the occurrence of horizontal displacement. This paper simultaneously considers the effects of dewatering and excavation, establishing a theoretical framework for predicting the drawdown and the horizontal displacement of the retaining structure. Firstly, a new method is established to calculate the drawdown caused by dewatering, deducing the numerical solution for the drawdown based on the unsteady seepage theory. Subsequently, a force balance equation for the water body element is established, based on the Rankine earth pressure theory, to derive a water and soil pressure calculation theory that takes into account seepage forces and drawdown. Meanwhile, this paper replaces the traditional Winkler foundation model with the Pasternak foundation model, deriving the bending differential equation and employing the finite difference method to calculate horizontal displacement. Compare the field monitoring data to verify the rationality of the theory. Analyze the calculation errors caused by neglecting drawdown and seepage forces, as well as the selection of foundation model. Additionally, further investigate the impacts of precipitation parameters and excavation parameters on the horizontal displacement and drawdown.

Keywords: drawdown; excavation and dewatering; retaining structure; seepage force; soil-water pressure distribution; unsteady-state seepage

1. Introduction

With the increase of excavation depth and the complexity of the surrounding environment, the deformation control of foundation pit engineering has become the focus of attention (Mangushev *et al.* 2016, Westermann *et al.* 2020, TerMartirosyan *et al.* 2022). Control of deformation in retaining structures is a crucial issue in foundation pit engineering. During the construction process, it is important to constantly monitor the horizontal displacement of the retaining structures to avoid safety accidents (Liu *et al*. 2015, Gotman and Gotman 2019, Jin *et al.* 2021, Rossella *et al.* 2021, Hyungjoon *et al.* 2022, Sun *et al.* 2022). Meanwhile, researchers have improved the stability of retaining wall structures by enhancing the materials used for the walls, while also conducting extensive studies on the consolidation of unsaturated soils (Liu *et al.* 2024, Satyanaga *et al.* 2024a, Gofar *et al.* 2022). As seepage is a critical factor affecting the stability of retaining walls and slopes, significant research efforts have also been dedicated to this area (Satyanaga *et al.* 2022, Satyanaga *et al.* 2024b).

Excavation-induced horizontal displacement of retaining structures is generally greater than that caused by dewatering. There has been no theoretical research on the horizontal displacement caused by dewatering, and it is unclear how much computational error can arise from ignoring the effects of dewatering. Dewatering causes a reduction in drawdown both inside and outside the pit, generating seepage forces that alter the distribution of water and soil pressures, this is the reason for the horizontal displacement caused by dewatering (Zeng *et al*. 2019). Zheng (2022) conducted on-site dewatering tests and found that the horizontal displacement caused by dewatering can reach 47% (Zeng *et al*. 2017) of the allowable deformation. Therefore, it is essential to establish a theoretical framework for calculating the horizontal displacement of retaining structures under the combined effects of excavation and dewatering, analyze the computational errors of horizontal displacement when ignoring dewatering, thereby guiding on-site construction and providing reference for existing theories.

The factors affecting the accuracy of horizontal displacement calculations for retaining structures primarily

*Corresponding author, Professor
E-mail: cshblast@163.com
[a]Ph.D. Student
[b]Senior Engineer
[c]Senior Engineer

ISSN: 2005-307X (Print), 2092-6219 (Online)

include two aspects. First, the inability to accurately calculate water-soil pressures. Some existing theories choose to ignore the impact of water pressure, assuming that the drawdown in both the active and passive zones drop below the excavation level (Perozzi *et al.* 2023, Han *et al*. 2024). However, in reality, the drawdown in the active zone is often much less than in the passive zone. Ignoring the water pressure difference between the two sides can lead to a significant underestimation. Another theoretical approach neglects the influence of drawdown when calculating water pressure, leading to issues with the distribution form of water-soil pressures, this approach does not consider the effects of seepage forces, resulting in errors in the horizontal displacement calculations (Huang *et al*. 2017). Second, the foundation model is overly simplified. Most existing studies use the Winkler elastic foundation beam model (Brandenberg *et al.* 2017), which has been shown to have low calculation precision. Pasternak (1954) proposed a new model that has been validated in tunnel displacement (Fu *et al.* 2023) and extensible reinforcement (Patra *et al.* 2015) calculations, demonstrating higher accuracy.

The distribution of drawdown both inside and outside the pit directly affects the calculation of water-soil pressures on both sides of the retaining structure, significantly impacting the calculations of horizontal displacement. However, the theoretical framework for calculating drawdown is quite inadequate. Existing theories can be primarily divided into two categories. The first category is drawdown prediction based on the Dupuit assumption (Hayek *et al.* 2024). This method uses steady-state seepage equations while neglecting the vertical component of seepage velocity (Loáiciga *et al.* 2020), providing only a rough estimate of drawdown. This theoretical model is overly simplified, resulting in low calculation accuracy and failing to account for temporal factors, making it unable to predict changes in drawdown over time (Rak *et al.* 2022). The second category involves drawdown calculation theories based on indoor experiments and fitting formulas (Yang and Zhao 2018). This method relies heavily on laboratory test results, which are significantly influenced by size effects. This study references the calculation theories for drawdown in dewatering wells (Neuman 1972, Teo *et al.* 2003, Chapuis *et al.* 2006, Chang and Yeh 2009) and utilizes the unsteady-state seepage equation, considering vertical seepage velocities and time effects (Stehfest 1970). Based on the equivalent large well method, a mathematical model is developed to calculate the temporal and spatial distribution of drawdown both inside and outside the pit.

To address these issues, this study proposes a new theory for calculating drawdown. By utilizing the obtained distribution of drawdown, the influence of seepage forces is considered to modify the existing soil and water pressure on both sides of the retaining structure. Additionally, the Pasternak two-parameter foundation model is introduced to derive the flexural differential equation, and the finite difference method is used to calculate the horizontal displacement. Finally, the calculation theory of horizontal displacement of retaining structure and the calculation theory of drawdown considering the influence of excavation and precipitation are established.

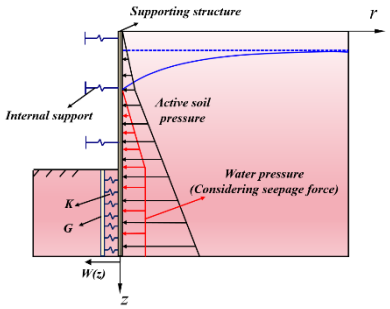

Fig. 1 Calculation model

2. Horizontal displacement of retaining structures under dewatering and excavation

Construct the calculation model for the horizontal displacement of the retaining structure, as shown in Fig. 1. It includes the foundation reaction coefficient k(kPa) and the shear modulus G(kPa). The basic assumptions are as follows:

1. The retaining structure is equivalently represented as a cylindrical beam with a diameter d and a flexural stiffness EI;

2. The retaining pile is closely attached to the foundation soil, and its deformation at the contact point is coordinated with the deformation of the foundation.

The bending differential equation for the retaining structure is as follows:

Free section

$$EI\frac{d^4w}{dz^4} + F_h - P_A B = 0 \tag{1}$$

Fixed section

$$EI\frac{d^4w}{dz^4} - GB\frac{d^2w}{dz^2} + KBw - P_A B + p_{wp}B = 0 \tag{2}$$

In the Eqs. (1) and (2), F_h represents the force exerted by the internal support (kN); B represents the calculation width of the horizontal force. G is referenced from the empirical formula proposed by the researchs (Tanahashi 2004). The value of K is referenced from the empirical formula proposed by the research (Vesic 1961). P_A is the active zone soil and water pressures, P_{wp} the passive zone water pressure.

Fig. 2 Retaining structure finite difference diagram

The pile is divided into n segments along its length, and each segment is l. The value of l is 0.5. As shown in Fig. 2.

The top and bottom are free boundaries, so the values of bending moment and shear force are both zero.

$$M_0 = EI\frac{d^2w_0}{dz^2} = 0 \tag{3}$$

$$Q_0 = EI\frac{d^3w_0}{dz^3} = 0 \tag{4}$$

$$M_n = EI\frac{d^2w_n}{dz^2} = 0 \tag{5}$$

$$Q_n = EI\frac{d^3w_n}{dz^3} = 0 \tag{6}$$

Calculation of horizontal displacement of the retaining pile by finite difference method

$$[K][w] = [F] \tag{7}$$

$$[K] = \begin{bmatrix} 2\alpha & -4\alpha & 2\alpha & & & & & & 0 \\ -2\alpha & 5\alpha & -4\alpha & \alpha & & & & & \\ \alpha & -4\alpha & 6\alpha & -4\alpha & \alpha & & & & \\ & \alpha & -4\alpha & 6\alpha & -4\alpha & \alpha & & & \\ & & \cdots & \cdots & \cdots & \cdots & & & \\ & & \alpha & -4\alpha-\gamma & 6\alpha+2\gamma+\eta & -4\alpha+\gamma & \alpha & & \\ & & & \alpha & -4\alpha-\gamma & 6\alpha+2\gamma+\eta & -4\alpha+\gamma & \alpha & \\ & & & & \alpha & -4\alpha-\gamma & 5\alpha+2\gamma+\eta & 2\alpha-\gamma & \\ 0 & & & & & 2\alpha & -4\alpha & 2\alpha+\eta & \end{bmatrix} \tag{8}$$

$$[w] = [w_0 \quad w_1 \quad w_2 \quad w_3 \quad \cdots \quad w_{n-3} \quad w_{n-2} \quad w_{n-1} \quad w_n] \tag{9}$$

$[F]$ is the external loads, including P_A, P_{wp} and F_h. $[K]$ is the horizontal stiffness matrix, and $[w]$ is the displacement at the pile nodes. The detailed derivation process is presented in Appendix A.

3. Drawdown distribution induced by foundation pit dewatering

3.1 Mathematical model and basic assumptions

The dewatering of the foundation pit creates a hydraulic gradient between the inside and outside of the pit, leading to seepage from the outside to the inside. The seepage zone is located between the bottom of the retaining structure and the impermeable layer, resulting in the drawdown both inside and outside the pit. The operation of foundation pit dewatering is similar to that of a dewatering well, which is why researchers have modeled the foundation pit as a large dewatering well. The diameter of the pit can be equivalently referenced based on these studies (Yu *et al.* 2022).

Fig. 3 shows the mathematical model for calculating the drawdown. Based on the principle of symmetry, calculations are performed for half of the foundation pit. S_w is the drawdown outside the pit near the retaining structure (m). r_w is the equivalent radius of the pit (m). b is the depth of the aquifer (m). ζ is the height of the infiltration zone (m). s is the drawdown outside the pit (m). h is the drawdown inside the pit (m). Q is pumping rate (m³/D).

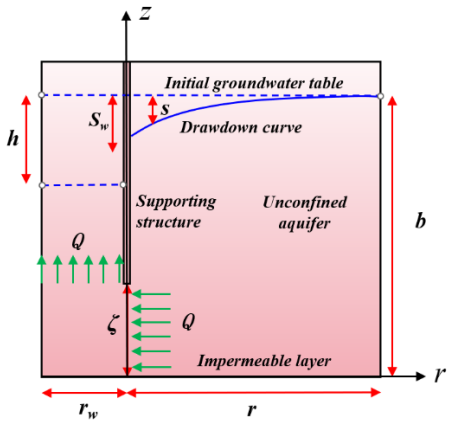

Fig. 3 Mathematical model for foundation pit dewatering

The basic assumptions are as follows:

1. The aquifer is uniform and anisotropic, and the impermeable layer is horizontal.
2. The initial water table is horizontally distributed.
3. The seepage follows Darcy's law.
4. The foundation pit is modeled as a large-diameter non-complete well.

3.2 Laplace domain solution for drawdown outside the pit

The basic equations for calculating drawdown are as follows

$$k_r\frac{\partial^2 s}{\partial r^2} + \frac{k_r}{r}\frac{\partial s}{\partial r} + k_z\frac{\partial^2 s}{\partial z^2} = S_s\frac{\partial s}{\partial t} \quad (0 < z < b, r_w < r < \infty) \tag{10}$$

The drawdown is zero at the moment of dewatering, the initial condition is

$$s(r,z,0) = 0 \tag{11}$$

The bottom is no-flow boundary

$$\frac{\partial s(r,z,t)}{\partial z}\Big|_{z=0} = 0 \tag{12}$$

The boundary condition for the free surface of the unconfined aquifer is (Teo *et al.* 2003, Chang and Yeh 2009)

$$k_z\frac{\partial s(r,z,t)}{\partial z}\Big|_{z=b} = -s_y\frac{\partial s(r,z,t)}{\partial t}\Big|_{z=b} \tag{13}$$

The drawdown is zero at infinity

$$s(r,z,t)\big|_{r\to\infty} = 0 \tag{14}$$

For constant flow dewatering, the boundary condition near the retaining structure is

$$s(r,z,t)\big|_{r\to\infty} = 0 \tag{15}$$

In Eq. (15), Ss is the equivalent specific storage (m^{-1}); k_r is the equivalent horizontal hydraulic conductivity (m/d); k_z is the equivalent vertical hydraulic conductivity (m/d); S_y is the specific yield.

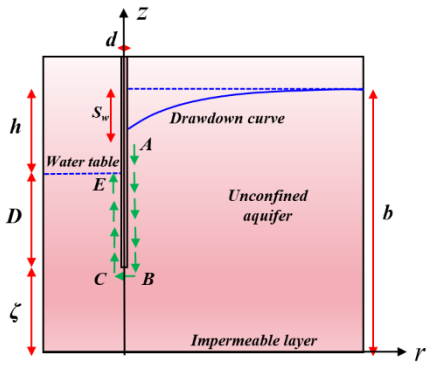

Fig. 4 Seepage path diagram

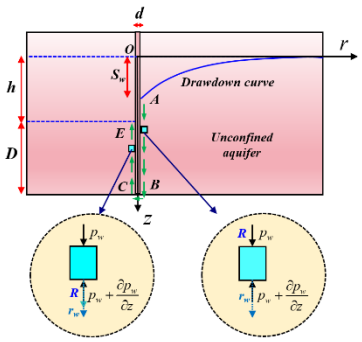

Fig. 5 Water body unit force analysis

Take the Laplace transform of the basic equations and boundary conditions to derive the Laplace domain solution $\tilde{s}$ for the external drawdown of the foundation pit

$$\tilde{s}(r,z,p)=\sum_{m=0}^{\infty}\lambda_m'(p)\frac{K_0\left[\sqrt{S_s p+C_m/k_r}\,r\right]}{\sqrt{S_s p+C_m/k_r}\,K_1\left[\sqrt{S_s p+C_m/k_r}\,r_0\right]}\cos(\beta_m z) \tag{16}$$

$$\lambda_m'(p)=\frac{Q\sin(\beta_m\zeta)}{\pi k_r r_w\zeta\, p\left[\cos(\beta_m\zeta)\sin(\beta_m L)+\beta_m\zeta\right]} \tag{17}$$

In Eq. (16), p is the Laplace variable. The Laplace inverse transform of $\tilde{s}(r,z,p)$ is performed using the Stehfest numerical inversion method, ultimately yielding the numerical solution for the spatial and temporal distribution of drawdown outside the foundation pit. $K_0(\cdot)$ is the modified Bessel function of second kind of order 0. $K_1(\cdot)$ is the modified Bessel function of second kind of order 1. The derivation process can be found in Appendix B.

3.3 Calculation of drawdown inside the pit

The relationship between the drawdown inside and outside the foundation pit can be referenced in this research (Wang *et al.* 2015). The seepage path is $A\to B\to C\to E$, as shown in Fig. 4. The average hydraulic gradient is

$$i_m=\frac{h-s_w}{2D+d+h-s_w} \tag{18}$$

In Eq. (18), h is the drawdown inside of the foundation pit. According to Darcy's law, the pumping rate Q can be expressed as

$$Q=2\pi k_r i_m(r_w+d)\zeta \tag{19}$$

Substitute Eq. (19) into Eq. (18) to obtain the pit internal drawdown h

$$h=\frac{2\pi k_r(r_w+d)\zeta(b-s_w)-Q(b-s_w+d-2\zeta)}{Q+2\pi k_r(r_w+d)\zeta} \tag{20}$$

By calculating the drawdown s_w from Section 3.2, and substituting it into Eq. (20), the drawdown inside the pit can be solved.

4. Water and soil pressure distribution considering drawdown and seepage force

Foundation pit drainage causes a drawdown in the water level, which affects water-soil pressure and generates seepage force acting on the retaining structure, ultimately influencing the horizontal displacement. Considering the seepage force and drawdown in the calculation of water-soil pressure, a force equilibrium analysis is conducted on the unit water body near the retaining structure, as shown in Fig. 5. Combining the boundary conditions, the calculation yields the water-soil pressure taking into account the seepage force and drawdown. pw represents the water pressure, and R is the viscous resistance of the soil to water, with the viscous resistance and seepage force being action-reaction forces.

Water pressure in active zone considering seepage force and drawdown

$$p_{wa}=\gamma_w\left(\frac{2D+d}{h-s_w+2D+d}\right)(z-s_w) \tag{21}$$

Water pressure in passive zone considering seepage force and drawdown

$$p_{wp}=\gamma_w\left(\frac{2(h-s_w+D)+d}{h-s_w+2D+d}\right)(z-h) \tag{22}$$

Soil pressure in active zone considering seepage force and drawdown

$$p_{sa}=k_a\gamma_s z-2c\sqrt{k_a}\qquad z<s_w \tag{23}$$

$$p_{sa}=k_a\left(\left(\gamma'+\gamma_w\frac{h-s_w}{h-s_w+2D+d}\right)\times z\right)-2c\sqrt{k_a}\qquad z>s_w \tag{24}$$

Soil pressure in passive zone considering seepage force and drawdown

$$p_{sp}=k_p\gamma_s z+2c\sqrt{k_p}\qquad z<h \tag{25}$$

$$p_{sp}=k_p\left(\left(\gamma'-\gamma_w\frac{h-s_w}{h-s_w+2D+d}\right)\times z\right)+2c\sqrt{k_p}\qquad z>h \tag{26}$$

The total distribution of water and soil pressure in the active and passive zones is obtained by superimposing water pressure and soil pressure

Table 1 Soil properties

Soil	Wet Density (g/cm^3)	water content (%)	void ratio (%)	Permeability Coefficient (m/s)	Compression Modulus (MPa)	Internal Friction Angle	Specific storage (m^{-1})	Water yield
Sandy Soil	1.91	0.39	0.4	1.55×10^{-4}	10.69	42	2.69×10^{-3}	0.4

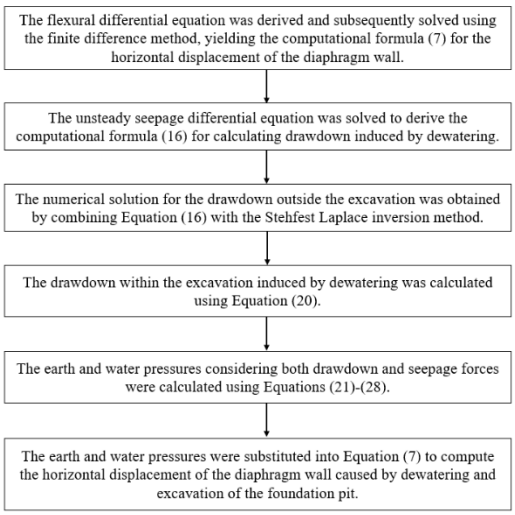

Fig. 6 Theoretical calculation flowchart

Fig. 7 Physical diagram of the experimental model tank

$$P_A = P_{wa} + P_{sa} \tag{27}$$

$$P_P = P_{wp} + P_{sp} \tag{28}$$

In (Eqs. (22)-(26)), γ_w is the unit weight of water, γ_s is the unit weight of soil, γ' is the buoyant unit weight of soil, c is the cohesion, k_a and k_p are the Rankine active earth pressure coefficient and passive earth pressure coefficient.

Detailed derivations shown in Appendix C. The computational theory flow of this study is illustrated in Fig. 6.

5. Analysis of calculation results

5.1 Model experiment

5.1.1 Overview of the model experiment

As shown in Fig. 7, the model box size is length× width× height=3.6m×1.1m×0.5m, with soil chamber length 2.8m and water chamber length 0.4m on both sides. The

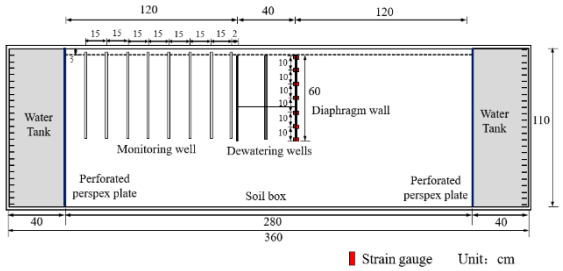

Fig. 8 Monitoring points layout diagram

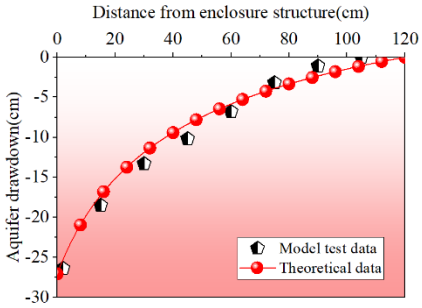

Fig. 9 Spatial comparison of drawdown

water chambers simulate constant-head recharge at soil boundaries in this test. The diaphragm wall was modeled using acrylic plates with elastic modulus 3.37 GPa, depth 60 cm, and thickness 4 mm. For pit dewatering, 2 dewatering wells with 2 peristaltic pumps were used. Through multiple pre-tests, the maximum pumping rate was determined as 1L/min to achieve specified dewatering depth. The dewatering wells used perforated PVC pipes with 16 mm inner diameter and 20 mm outer diameter. Sandy soil was used for testing, with properties shown in Table 1. In this model test, the infiltration zone height was 48 cm, with water level at 100 cm. One-time dewatering to specified height was conducted, with pre-excavation dewatering time 120min. Excavation was then performed in 4 layers, each 8 cm deep. Monitoring point layout is shown in Fig. 8.

5.1.2 Experimental validation of the drawdown and diaphragm wall displacement theory

As shown in Fig. 9, the theoretical spatial distribution of drawdown closely matches the experimental results, both showing a "funnel-shaped" pattern where drawdown decreases with distance from the diaphragm wall.

Fig. 10 presents the temporal distribution at r=2 cm, 30 cm, 60 cm, and 90 cm locations. Both theoretical and measured drawdown exhibit the same trend: initial rapid increase, followed by gradual growth, and eventual stabilization.

Table 2 Geotechnical properties of soil layers

soil layers	Thickness/m	Soil density (kN/m^3)	Buoyant density (kN/m^3)	Angle of internal friction	Cohesion /(kPa)	Poisson's ratio
Plain fill	1	18.5	17.8	12	13	0.3
Residual sandy clay	6.2	21.5	20.1	15	24	0.3
Fully weathered granite	4.1	20.8	19.5	18	28	0.28
Granular strongly weathered granite	18.5	22	20.5	28	20	0.25
Fragmented strongly weathered granite	6.2	24.2	22	29	22	0.22

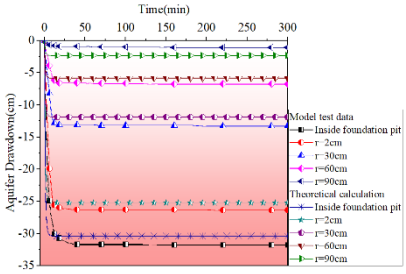

Fig. 10 Temporal comparison of drawdown

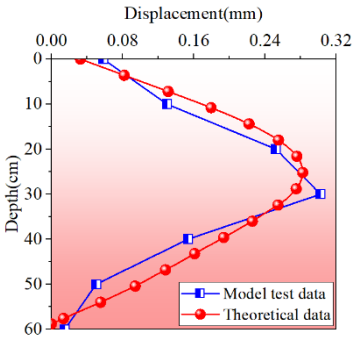

Fig. 11 Comparative analysis of horizontal displacement

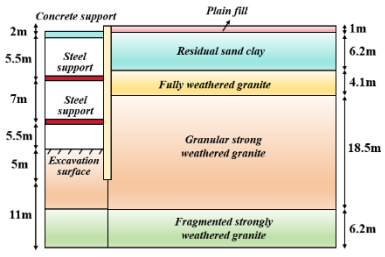

Fig. 12 Engineering geological conditions

Fig. 11 shows that the theoretical and experimental horizontal displacements of the diaphragm wall both display a "bulging" distribution, with maximum displacement occurring near 30 cm. The close agreement between theoretical and measured patterns demonstrates the validity of the proposed calculation method.

5.2 Project overview

Taking the subway foundation pit project in Xiamen as the background, the dimensions are 231.6 m (length) × 20 m (width) × 20 m (depth). The diameter of the retaining

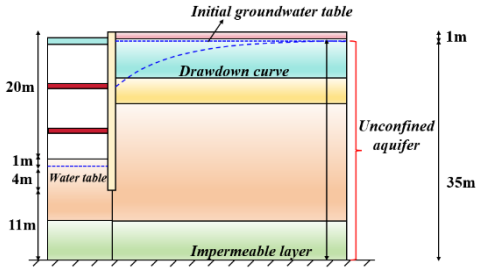

Fig. 13 Aquifer conditions

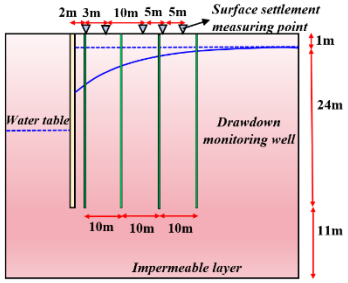

Fig. 14 Layout of monitoring points

structure is 1.2 m. The water level is lowered by adopting dewatering methods within the foundation pit. The aquifer is a unconfined aquifer with a depth of 35 m. The pumping rate is 18000 m^3/d (from 18 wells, with a single well pumping rate of 1,000 m^3/d). Monitoring wells are set at distances of 2 m, 10 m, 20 m, and 30 m from the retaining structure. The support structure and soil layer conditions are hown in Fig. 12, the aquifer conditions are shown in Fig. 13. The locations of the monitoring points are shown in Fig. 14. The mechanical properties of the soil layers are shown in Tables 2 and 3. The hydrological properties of the soil are represented by equivalent parameters (Zhang *et al.* 2022). The soil parameters used in the final theoretical calculations are presented in Tables 2 and 4. The equivalent calculation formulas for geotechnical properties can be found in references (Qiao *et al.* 2024, Zhang *et al.* 2006, Liu *et al.* 2021, Mu *et al.* 2020), while the equivalent calculation formulas for hydraulic properties can be found in references (Wang *et al.* 2021, Huo *et al.* 2009, Fetter 2001, Bear 1979).

5.3 Theoretical validation

5.3.1 Theoretical validation of drawdown calculation

Table 3 Hydrological properties of soil layers\

Soil layers	Thickness/m	Horizontal permeability coefficient (m/d)	Vertical permeability coefficient (m/d)	Water storage capacity (m^{-1})	Water content
Plain fill	1	0.15	0.15	9×10^{-4}	0.02
Residual sandy clay	6.2	0.1	0.1	9×10^{-4}	0.05
Fully weathered granite	4.1	0.3	0.28	8.11×10^{-5}	0.18
Granular strongly weathered granite	18.5	0.5	0.46	8.54×10^{-5}	0.17
Fragmented strongly weathered granite	6.2	3	2.8	9.6×10^{-5}	0.15

Table 4 Theoretical calculation parameters of drawdown

Soil layers	Thickness/m	Horizontal permeability coefficient (m/d)	Vertical permeability coefficient (m/d)	Water storage capacity (m^{-1})	Water content
Equivalent parameters	36	0.85	0.29	2.3×10^{-4}	0.146

The validity of the drawdown calculation theory is verified by comparing field monitoring data from both temporal and spatial distribution perspectives. In terms of temporal distribution, as shown in Fig. 15, data from the monitoring well located 2 m away from the pit is compared. The drawdown initially increases rapidly, then gradually slows down, with a maximum drawdown of approximately 6.28 m, and the timings are quite similar. For spatial distribution, as shown in Fig. 16, drawdown monitoring data from the 80th day of dewatering is compared across four monitoring wells. As shown in Fig. 16, the spatial distribution of drawdown exhibits a "funnel-shaped" pattern, with the maximum drawdown occurring adjacent to the diaphragm wall. Theoretical predictions demonstrate errors within 5% for all monitoring points. The theoretical calculation results closely match the field monitoring results, further confirming the validity of the theory

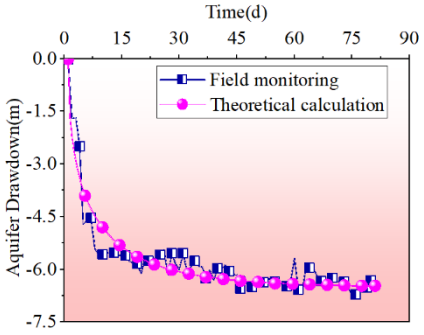

Fig. 15 Time distribution of drawdown

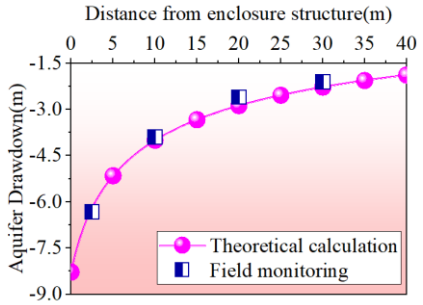

Fig. 16 Spatial distribution of drawdown

5.3.2 Theoretical validation of horizontal displacement of retaining structures

The calculation results of this paper are compared with field monitoring results to verify the rationality of the theory. To study the effects of dewatering and the impact of foundation models, this paper considers different distributions of water and soil pressure, as well as the influence of different foundation models on the horizontal displacement of retaining structures, using four calculation modes. Mode 1 considers the impact of pit dewatering, using a water and soil pressure distribution that accounts for drawdown and seepage forces, with the foundation model selected as the Winkler model. Mode 2 adopts a traditional method of calculating water and soil pressure, neglecting the effects of drawdown and seepage forces, and also uses the Winkler model. Mode 3 employs the traditional calculation method for water and soil pressure, ignoring drawdown and seepage forces, with the foundation model chosen as the Pasternak model. Mode 4 assumes dry soil layers, neglecting the effects of water pressure and seepage forces, and similarly uses the Pasternak model for the foundation. Fig. 17 shows these comparisons.

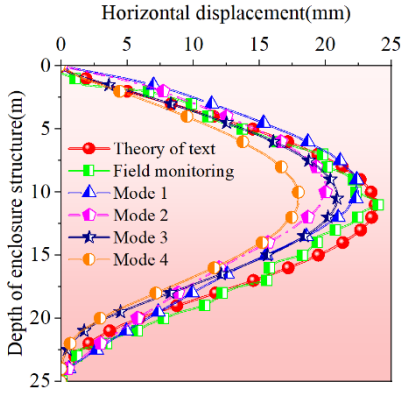

Fig. 17 Comparison of horizontal displacement of retaining structures

As shown in Fig. 17, the calculation method in this paper exhibits the highest compatibility with field monitoring results. The maximum horizontal displacements are 23.75 mm and 23.99 mm, with an error of only 1%. In terms of depth, the trend of horizontal displacement is largely consistent between the theoretical and field data, with the maximum displacement occurring at a depth of 11m. This demonstrates that the research methods used in this study are more comprehensive and accurate.

Comparing Mode 1 with the theoretical method in this study, the maximum displacement depth calculated using the Winkler foundation model is smaller, differing from field data by 2 m, which represents an error of 16.7%. The maximum horizontal displacement differs by 1.45 mm, with an error of 6.1%. This indicates that the Winkler foundation model has lower accuracy compared to the Pasternak two-parameter model.

Comparing Mode 2 with the theoretical method in this study, which uses a traditional water and soil pressure calculation method and neglects the effects of drawdown and seepage forces, the calculated horizontal displacement is underestimated, differing from field data by 3.95 mm, resulting in an error of 14.5%. The location of the maximum horizontal displacement differs by 2 m from the field measurements, with an error of 16.7%. This indicates that neglecting drawdown and seepage forces leads to an underestimation of the calculated results.

Analyzing Mode 3, the traditional water and soil pressure calculation method is used, neglecting the effects of drawdown and seepage forces, while employing the Pasternak two-parameter foundation model. The calculated horizontal displacement is 2.86 mm smaller than the theoretical calculation in this study, with an error of 12.1%. However, compared to Mode 2, the results are closer to the field data. This suggests that the selection of the Pasternak two-parameter foundation model, along with consideration of drawdown and seepage forces, can improve the accuracy of horizontal displacement calculations.

Comparing Mode 4 with the theoretical results in this study, when neglecting the effects of water pressure and seepage forces and only considering the influence of soil pressure, the calculated maximum displacement is only 17.5 mm. This differs from the theoretical result by 6.25 mm, resulting in an error of 26.3%. This indicates that the effects of water pressure and seepage forces are significant and cannot be ignored. In summary, when calculating the horizontal displacement caused by excavation and dewatering, it is essential to fully consider the effects of drawdown and seepage forces. Traditional calculation methods have significant errors. The Pasternak foundation model offers higher computational accuracy.

5.3.3 Distribution pattern of drawdown

As shown in Fig. 18, the drawdown gradually increases, with the increase rate slowing over time. The drawdown can be roughly divided into two phases with the 20d mark as a boundary: a rapid increase phase and a slow increase phase. By 80 days, the drawdown reaches its maximum value of 21.03 m. Due to the barrier effect of the retaining structure on the flow path, the drawdown inside the pit is significantly greater than that outside the pit.

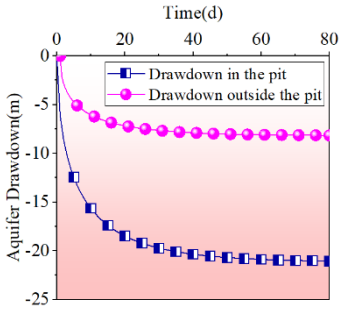

Fig. 18 Variation of drawdown over time

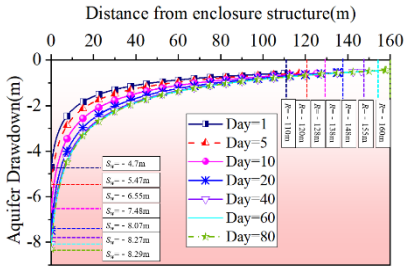

Fig. 19 Spatial and temporal variation of drawdown outside the pit

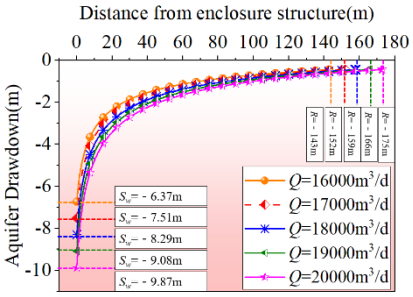

Fig. 20 Influence of flow rate on spatial distribution of drawdown outside the pit

As shown in Fig. 19, the drawdown decreases as the distance from the retaining structure increases. The longer the dewatering time, the greater the influence range, with a maximum impact range of up to 160 m. As dewatering progresses, the drawdown near the diaphragm wall shows significant reduction, while the decrease becomes progressively smaller at increasing distances from the wall.

5.3.4 Influence of pumping rate on drawdown

As shown in Fig. 20, with dewatering rates of 16,000 m³/d, 17,000 m³/d, 18,000 m³/d, 19,000 m³/d, and 20,000 m³/d, the pumping rate increases the drawdown and expands the influence range of dewatering. The impact is more significant near the retaining structure, where the drawdown increases from 6.37 m to 9.87 m (a difference of 3.5 m). representing 42.2% of the field-observed drawdown magnitude (Q=18000 m³/d), which demonstrates the significant influence of pumping rate variation on drawdown development. As the distance from the retaining structure increases, the difference in drawdown values decreases. The influence range of dewatering increases from 143 m to 175 m.

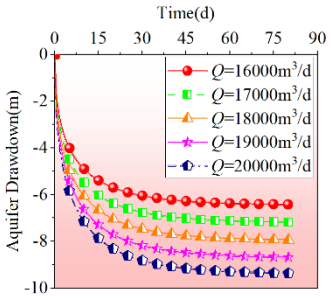

Fig. 21 Influence of pumping rate (outside the pit)

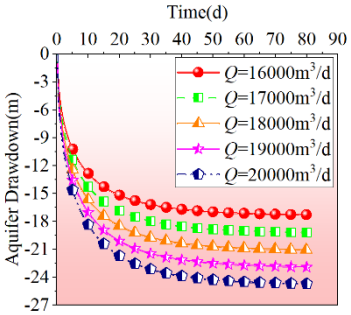

Fig. 22 Influence of pumping rate (inside the pit)

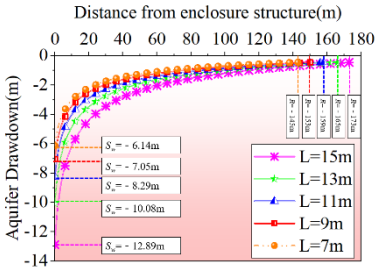

Fig. 23 Influence of infiltration zone depth

As shown in Fig. 21 and Fig. 22, under different pumping rate Q, the drawdown outside the pit increases from 6.37 m to 9.87 m, accounting for 42.2% of the field conditions. The drawdown inside the foundation pit increases from 17.28 m to 24.71 m, accounting for 35.4% of the field conditions. The drawdown analysis in Figs. 16 and 17 examines variation of maximum drawdown and computational errors under standard conditions, clearly demonstrating the influence of pumping rate on drawdown.

5.3.5 Influence of infiltration zone depth on drawdown

As shown in Fig. 23, with infiltration zone depths of 7 m, 9 m, 11 m, 13 m, and 15 m, the depth of the infiltration zone can increase the drawdown and expand the influence range of dewatering. The impact near the retaining structure is more significant, with the drawdown increasing from 6.14 m to 12.89 m. As the distance from the retaining structure increases, the difference in drawdown values decreases. The influence range of dewatering expands from 145 m to 173 m.

As shown in Figs. 24 and 25, under different infiltration zone depths, the drawdown outside the foundation pit increases from 6.14 m to 12.89 m (a difference of 6.75 m). representing 81.4% of the field-observed drawdown

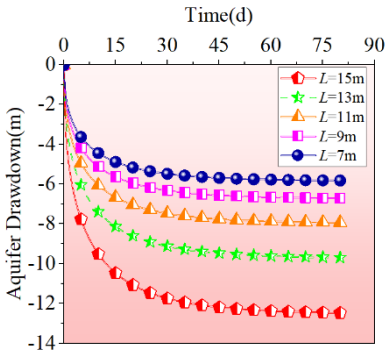

Fig. 24 Influence of infiltration zone (outside the pit)

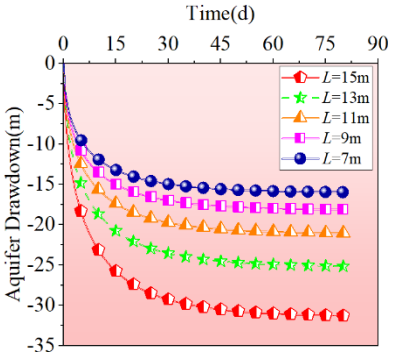

Fig. 25 Influence of infiltration zone (inside the pit)

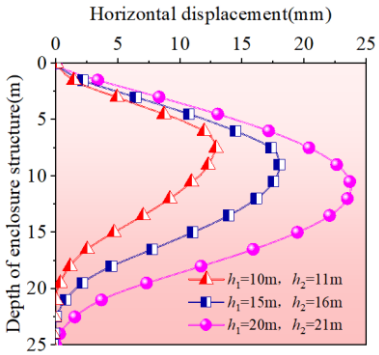

Fig. 26 Influence of dewatering and excavation depth

magnitude (L=11 m). Meanwhile, the drawdown inside the foundation pit increases from 15.94 m to 31.29 m, accounting for 72.9% of the field conditions. Varying L only increases the magnitude of drawdown but does not affect the variation trend of the drawdown curve.

5.3.6 Influence of excavation and dewatering depth on displacement

The study investigates the variation of horizontal displacement of retaining structures during dewatering and excavation of a foundation pit. Excavation depths h_1 are 10 m, 15 m, and 20 m, with corresponding drawdown inside the pit h_2 of 11 m, 16 m, and 21 m, resulting in external drawdown of 6.9 m, 7.8 m, and 8.2 m respectively. The specific pattern of horizontal displacement is illustrated in Fig. 26. As excavation and dewatering progress, the horizontal displacement gradually increases. The depth of maximum horizontal displacement also increases, and the

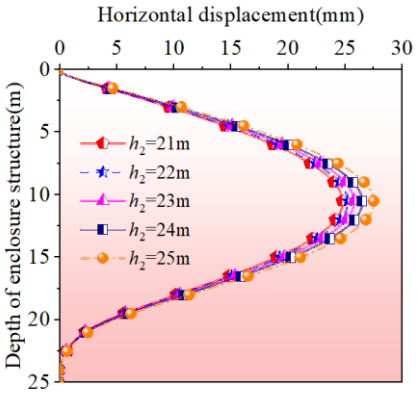

Fig. 27 Influence of dewatering depth

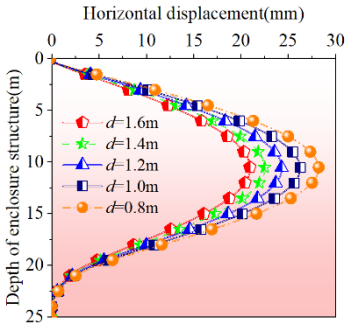

Fig. 28 Influence of retaining structure diameter

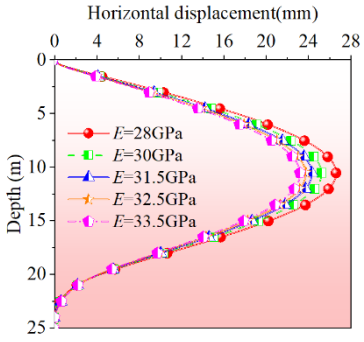

Fig. 29 Influence of retaining structure material

deformation pattern of the retaining structures remains consistent, characterized by a "bulging" shape. As shown in Fig. 27, with a fixed excavation depth h_1 of 20 m, the pit dewatering depths h_2 are 21 m, 22 m, 23 m, 24 m, and 25 m. A greater dewatering depth h_2 results in larger horizontal displacement. Different pit dewatering depths h_2 have minimal impact on the location of maximum horizontal displacement of the retaining structures.

5.3.7 Influence of retaining structure properties on horizontal displacement

As shown in Fig. 28, with a fixed excavation depth of 20m and dewatering depth of 21 m, changing only the diameter d of the retaining structure results in a decrease in horizontal displacement as the diameter increases. The maximum horizontal displacement differs by 7.24 mm, covering 30.1% of the site conditions, indicating that increasing the diameter can significantly control horizontal displacement.

As shown in Fig. 29, with a fixed excavation depth of 20 m and dewatering depth of 21 m, changing only the material of the retaining structure to C25, C30, C35, C40 and C45 concrete respectively. As the concrete strength increases, the horizontal displacement decreases, suggesting that increasing the strength of the retaining structure can significantly reduce deformation.

6. Conclusions

A theoretical framework for accurate prediction of both drawdown in unconfined aquifers and retaining structure displacements induced by dewatering and excavation is proposed, with its validity systematically verified through field monitoring and physical model testing. The main conclusions are as follows:

- This paper presents a method for calculating the drawdown of drawdown inside and outside the foundation pit. Theoretical results were compared with field monitoring data and model test results to verify the rationality of the drawdown prediction theory. With the progression of dewatering, the drawdown initially increases rapidly, then grows at a slower rate, and eventually stabilizes. The theoretical calculations demonstrate excellent agreement with field monitoring data and model test data in terms of drawdown evolution trends.
- This paper builds on traditional theories of water and soil pressure by incorporating seepage forces and considering the impact of drawdown. This approach ensures that the water and soil pressure during the calculation of horizontal displacement aligns more closely with actual conditions, thereby improving the accuracy of horizontal displacement calculations.
- This paper employs the Pasternak foundation model, combined with a soil-water pressure calculation theory that considers seepage forces and drawdown, to derive the bending differential equation. Using the finite difference method, the horizontal displacement of the retaining structure is calculated and compared with field monitoring results. The maximum horizontal displacements are 23.75 mm and 23.99 mm, with an error of only 1%. Both theoretical calculations and field monitoring demonstrate that the horizontal displacement of the diaphragm wall follows a "bulging" distribution pattern, with remarkably similar variation trends between the two datasets. The horizontal displacement along the depth direction shows close agreement, demonstrating that the proposed calculation theory has high accuracy.
- Neglecting the effects of seepage forces, drawdown, and water pressure leads to an underestimation of horizontal displacement calculations. The results from the Winkler model are typically lower than those from the Pasternak model, and the Winkler model exhibits significant errors in predicting the distribution of horizontal displacement with depth. The theoretical approach proposed in this study

demonstrates a computational error of 1%, while the horizontal displacement errors under four different modes are 1%, 6.1%, 16.7%, 12.1%, and 26.1% respectively, further validating the precision of the present theory.

• The drawdown inside the pit is greater than that outside. Increasing the pumping rate and the height of the infiltration zone can enhance the drawdown and the range of dewatering effects. The greater the excavation depth and dewatering depth, the smaller the diameter of the retaining structure and the lower its strength, resulting in larger horizontal displacements.

Discussion

The theoretical approach presented in this study accurately predicts both the drawdown induced by foundation pit dewatering and the corresponding horizontal displacement of diaphragm walls. The model comprehensively accounts for the effects of drawdown and seepage forces on both groundwater lowering and wall displacement. By incorporating the Pasternak two-parameter model, the proposed method improves upon existing theories for drawdown and displacement calculations, ultimately achieving precise prediction of drawdown and wall displacement. However, this theoretical framework is only applicable to unconfined aquifers and cannot be extended to confined aquifer conditions, which will be the focus of subsequent research phases.

References

Bear, J. (1979), "Hydraulics of Groundwater", *McGraw-Hill*, New York.

Brandenberg, J.S., Mylonakis, G. and Stewart, P.J. (2017), "Approximate solution for seismic earth pressures on rigid walls retaining inhomogeneous elastic soil", *Soil Dyn. Earthq. Eng*., **97**(2017), 468-477. https://doi.org/10.1016/j.soildyn.2017.03.028.

Chang, Y.C., Chen, G.Y. and Yeh, H.D. (2011), "Transient flow into a partially penetrating well during the constant-head test in unconfined aquifers", *J. Hydraul. Eng*., **137**(9), 1054-1063. https://doi.org/10.1061/(ASCE)HY.1943-7900.0000392.

Chang, Y.C., and Yeh, H.D. (2009), "New solutions to the constant-head test performed at a partially penetrating well", *J. Hydrol*., **369**(1-2), 90-97. https://doi.org/10.1016/j.jhydrol.2009.02.016.

Chapuis, R.P., Bélanger, C. and Chenaf, D. (2006), "Pumping test in a confined aquifer under tidal influence", *Ground. Water.*, **44**(2), 300-305. https://doi.org/10.1111/j.1745-6584.2005.00139.x.

Chen, C.S. and Chang, C.C. (2003), "Well hydraulics theory and data analysis of the constant head test in an unconfined aquifer with the skin effect", *Water. Resour. Res.*, **39**(5), 63-69. https://doi.org/10.1029/2002WR001516.

Fetter, C.W. (2001), "Applied Hydrogeology (4th ed.)", *Prentice Hall*, New Jersey.

Fu, Y.B., Wang, B.L., Wu, H., Chen, X.S., Sun, X.H., Bian, Y.W. and Shen, X. (2023), "Theoretical analysis on horizontal rectification of tunnel near deep foundation pit by grouting", *Tunn. Undergr. Sp. Tech.*, **133**. https://doi.org/10.1016/j.tust.2022.104977.

Gofar, N. and Satyanaga, A. (2022), "Sustainable retaining structure incorporating recycled concrete aggregate", *Indones. Geotech J.* https://doi.org/10.56144/igj.v1i3.32.

Gotman, A.L. and Gotman, Y.A. (2019), "Numerical analysis of the shorings of deep foundation pits with regard for the soil solidification", *Soil. Mech. Found. Eng.*, **56**(4), 225-231. https://doi.org/10.1007/s11204-019-09595-6.

Han, M., Chen, X.S. and Jia, J.Q. (2024), "Analytical solution for displacement-dependent 3D earth pressure on flexible walls of foundation pits in layered cohesive soil", *Acta. Geotech.*, https://doi.org/10.1007/s11440-024-02226-x.

Hayek, M. (2024), "Steady-state flow under surface recharge through unconfined aquifer with depth-decaying hydraulic conductivity: Analytical results", *J. Hydrol.*, **638**(2024), 131469-131469. https://doi.org/10.1016/J.JHYDROL.2024.131469.

Huang, M., Liu, X.R., Zhang, N.Y. and Shen, Q.W. (2017), "Calculation of foundation pit deformation caused by deep excavation considering influence of loading and unloading", *J. Cent. South. Univ*., **24**(9), 2164-2171. https://doi.org/10.1007/s11771-017-3625-3.

Hyungjoon, S., Yang, Z. and Cheng, C. (2022), "Displacement mapping of point clouds for retaining structure considering shape of sheet pile and soil fall effects during excavation", *J. Geotech. Geoenviron*., **148**(5). https://doi.org/10.1061/(ASCE)GT.1943-5606.0002800.

Jin, H.L., Zhang, G. and Yang, Y.S. (2021), "Experimental and numerical study on behavior of retaining structure with limited soil", *Geomech. Eng*., **26**(1), 77-88. https://doi.org/10.12989/gae.2021.26.1.077.

Liu, J.G., Zhou, D.D. and Liu, K.W. (2015), "A mathematical model to recover missing monitoring data of foundation pit", *Geomech. Eng*., **9**(3), 275-286. https://doi.org/10.12989/gae.2015.9.3.275.

Liu, L.L., Wu, R.G., Congress, S.S.C., Du, Q.W., Cai, G.J. and Li, Z. (2021), "Design optimization of the soil nail wall-retaining pile-anchor cable supporting system in a large-scale deep foundation pit", *Acta Geotech.*, **16**(7), 2251-2274, http://dx.doi.org/10.1007/s11440-021-01154-4.

Liu, Y., Ma, R.C., Zhu, Y.Y., Yi, X.T., Satyanaga, A., Dai, G.L. and Zhai, Q. (2024), "Oedometer study regarding the consolidation behavior of Nanjing soft clay", *Appl. Sci.*, **14**(16), 7339. https://doi.org/10.3390/APP14167339.

Loáiciga, A.H. (2020), "Seepage face in steady-state groundwater flow between two water bodies", *J. Hydrol. Eng*., **25**(9). https://doi.org/10.1061/(ASCE)HE.1943-5584.0001997.

Luo, Y., Gong, X.N. and Wu, R.Q. (2007), "New method for calculation of water-earth pressure on foundation pit considering groundwater seepage", *J. Zhejiang Univ.,* (1), 157-160. https://doi.org/10.1360/yc-007-0745.

Mangushev, R.A., Osokin, A.I. and Garnyk, L.V. (2016), "Experience in preserving adjacent buildings during excavation of large foundation pits under conditions of dense development", *Soil. Mech. Found. Eng*., **53**(5), 291-297. https://doi.org/10.1007/s11204-016-9401-9.

Mu, Y.J., Yuan, D.J., Wang, J., Liu, B. and Wang, C.Z. (2020), "Calculation model of the long-term settlement in the weak watery stratum considering leakage of shield tunnel", *China Civ. Eng. J.*, **53**, 7-12, https://doi.org/10.15951/j.tmgcxb.2020.s1.002.

Neuman, S.P. (1972), "Theory of flow in unconfined aquifers considering delayed response of the water table", *Water. Resour. Res.*, **8**(4), 1031-1045. https://doi.org/10.1029/WR008i004p01031.

Pasternak, P.L. (1954), "On a new method of an elastic foundation by means of two foundation constants", Gosudarstvennoe Izdatelstvo Literaturi Po Stroitelstuve I Arkhitekture.

Patra, S. and Shahu, T.J. (2015), "Behaviour of extensible reinforcement resting on non-linear Pasternak subgrade

subjected to oblique pull", *Géotechnique.*, **65**(9), 770-779. https://doi.org/10.1680/geot.14.P.233.

Perozzi, D. and Puzrin, A.M. (2023), "Limit-state solutions for the active earth pressure behind walls rotating about the base", *Géotechnique.*, **2023**, 1-12. https://doi.org/10.1680/JGEOT.23.00093.

Qiao, S.F., Chen, D.L., Cai, Z.Y., Liu, Y.Q., Meng, F. and Tan, J.K. (2024), "Analysis of active earth pressure of flexible retaining wall considering multiple factors", *J. Build. Struct.*, 1-14. https://doi.org/10.14006/j.jzjgxb.2024.0089.

Rak, M.C. and Bum, G.K. (2022), "Optimum interval of artificial groundwater recharge wells, considering injection rate and economic feasibility", *Geosci. J.*, **7**(1), 77-87. https://doi.org/10.1007/S12303-022-0019-9.

Rossella, B. and Antonio, B., (2021), "Effect of deep excavations and deformable retaining structures on neighboring buildings: A case study", *Eng. Fail. Anal.*, **122**(2021). https://doi.org/10.1016/J.ENGFAILANAL.2021.105269.

Satyanaga, A., Moon, S.W., Wijaya, M., Irawann, S. and Kim, J. (2022), "Factor of safety variations of residual soil slopes under rainfall loading", *Proceedings of the 5th International Conference on Numerical Modelling in Engineering (NME 2022).*

Satyanaga, A., Moon, S.W., Zhang, D. and Kim, J. (2024b), "Geostatistical Analysis for Mapping of Soil Properties", (Ed., Rotaru, A.), Knowledge Transfer in the Sustainable Rehabilitation and Risk Management of the Built Environment, KNOW-RE-BUILT 2021, Springer Series in Geomechanics and Geoengineering, Springer, Cham. https://doi.org/10.1007/978-3-031-43455-6_17.

Satyanaga, A., Wijaya, M., Hamdany, A.H., Moon, S.W. and Kim, J. (2024a), "8 - Green retaining structure utilizing recycled concrete aggregate", Elsevier Ltd.

Stehfest, H. (1970), "Algorithm 368: Numerical inversion of Laplace transforms [D5]", *Commun. Acm.*, **13**(1), 47-49. https://doi.org/10.1145/361953.361969.

Sun, Y., Che, Y.F., Gu, Z.X., Wang, R.C. and Fan, Y.W. (2022), "Measured structural response of a long irregular pit constructed using a top-down method", *Geomech. Eng.*, **31**(5), 489-503. https://doi.org/10.12989/gae.2022.31.5.489.

Tanahashi, H. (2004), "Formulas for an infinitely long bernoulli-euler beam on the pasternak model", *Soils. Found.*, **44**(5), 109-118. https://doi.org/10.3208/sandf.44.5.

Teo, H., Jeng, D., Seymour, B., Barry, D.A. and Li, L. (2003), "A new analytical solution for water table fluctuations in coastal aquifers with sloping beaches", *Adv. Water. Resour.*, **26**(12), 1239-1247. https://doi.org/10.1016/j.advwatres.2003.08.004.

TerMartirosyan, Z.G., TerMartirosyan, A.Z. and Vanina Y.V. (2022), "Mathematical analysis for the evaluation of settlement and load-bearing capacity of a soil base adjacent to an excavation pit", *Axioms.*, **11**(8), 353-353. https://doi.org/10.3390/axioms11080353.

Vesic, A.S. (1961), "Bending of beams resting on isotropic elastic solids", *J. Eng. Mech. Division*, **87**(2), 35-53. https://doi.org/10.1061/JMCEA3.0000212.

Wang, J.H., Tao, L.J., Han, X. and Zhou, H.L. (2015), "Effect of suspended curtain depth into stratum of discharge rate and its optimun design", *J. Beijing. Univ. Tech.*, **41**(9), 1390-1398. https://doi.org/10.11936/bjutxb2015010006.

Wang, J.X., Feng, B., Liu, Y., Wu, L.G., Zhu, Y.F., Zhang, X.S., Tang, Y.Q. and Yang, P. (2012), "Controlling subsidence caused by de-watering in a deep foundation pit", *Bull. Eng. Geol. Environ.*, **71**(3), 545-555. https://doi.org/10.1007/s10064-012-0420-0.

Westermann, K., Meier, J. and Pitteloud, L. (2020), "Excavation pit and foundation of a research center", *Bautechnik.*, **97**(12), 878-885. https://doi.org/10.1002/bate.202000062.

Yang, Q.Y. and Zhao, B.M. (2018), "Experimental and theoretical study on the surface subsidence by dewatering of foundation pit in phreatic aquifer", *Chin. J. Rock. Mech. Eng.*, **37**(6), 1506-1519. https://doi.org/10.13722/j.cnki.jrme.2017.1611.

Yu, J., Yang, X.X., Deng, P.B. and Chen, W.B. (2022), "Analytical solution for a steady seepage field of a foundation pit in layered soil", *Int. J. Geomech.*, **22**(10). https://doi.org/10.1061/(ASCE)GM.1943-5622.0002496.

Zeng, C.F., Zheng, G. and Xue, X.L. (2017), "Wall deflection induced by pre-excavation dewatering in large-scale excavations", *Chin. J. Geotech. Eng.*, **39**(6), 1012-1021. https://doi.org/10.11779/CJGE201706006.

Zeng, C.F., Zheng, G., Zhou, X.F., Xue, X.L. and Zhou, H.Z. (2019), "Behaviours of wall and soil during pre-excavation dewatering under different foundation pit widths", *Comput. Geotech.*, **115**, , 103169. https://doi.org/10.1016/j.compgeo.2019.103169.

Zhang, S., Zhang, D.S. and Feng, G.R. (2022), "Quantitative evaluation and planning method of shallow surface water response in multi-face mining—Case study regarding Zhuanlongwan coal mine", *J. Clean. Prod.*, **373**(2022), https://doi.org/10.1016/J.JCLEPRO.2022.133830.

Zhang, Y.D. and Gong, X.N. (2006), "Improvement on basal heave stability analysis for excavations in soft clay", *Chin. J. Geotech. Eng.*, 1378-1382. https://doi.org/10.3321/j.issn:1000-4548.2006.z1.015.

Zheng, G. (2022), "Method and application of deformation control of excavations in soft ground", *Chin. J. Geotech. Eng.* **44**(1), 1-36+201.

CC

Appendix A

Let $\alpha = EI/l^4$, $\gamma = GB/l^2$, $\eta = kB$.

Perform finite differences on the free segment equation Eq. (1) and the fixed segment equation Eq. (2).

$$\alpha\left[w_{i+2} - 4w_{i+1} + 6w_i - 4w_{i-1} + w_{i-2}\right] + F_h - P_A B = 0 \quad \text{(A.1)}$$

$$\begin{aligned} &\alpha w_{i+2} - (4\alpha + \gamma) w_{i+1} + (6\alpha + 2\gamma + \eta) w_i \\ &-(4\alpha + \gamma) w_{i-1} + \gamma w_{i-2} - P_A B + p_{wp} B = 0 \end{aligned} \quad \text{(A.2)}$$

Perform finite differences on the boundary conditions.

$$M = \frac{EI}{l^2}\left(w_{i+1} - 2w_i + w_{i-1}\right) \quad \text{(A.3)}$$

$$Q = \frac{EI}{2l^3}\left(w_{i+2} - 2w_{i+1} + 2w_{i-1} - w_{i-2}\right) \quad \text{(A.4)}$$

Taking $i = 0$, combining the top moment and shear force boundary conditions yields

$$w_{-1} = 2w_0 - w_1 \quad \text{(A.5)}$$

$$w_{-2} = 4w_0 - 4w_1 + w_2 \quad \text{(A.6)}$$

Taking $i = n$, combining the bottom moment and shear force boundary conditions yields

$$w_{n+1} = 2w_n - w_{n-1} \quad \text{(A.7)}$$

$$w_{n+2} = 4w_n - 4w_{n-1} + w_{n-2} \quad \text{(A.8)}$$

Taking $i = 0,1,2,\cdots,m$ for Eq. (A.1) and substituting Eq. (A.5) and Eq. (A.6), taking $i = n, n-1, n-2, \cdots, m$ for Eq. (A.2) and substituting Eq. (A.7) and Eq. (A.8), and Eq. (7) can be derived.

Appendix B

Applying the Laplace transform to the basic equations and boundary conditions.

Applying the Laplace transform to Eq. (10) and using the initial condition, that is

$$k_r \frac{\partial^2 \tilde{s}}{\partial r^2} + \frac{k_r}{r}\frac{\partial \tilde{s}}{\partial r} + k_z \frac{\partial^2 \tilde{s}}{\partial z^2} = S_s p\tilde{s} \quad \left(0 < z < b, r_0 < r < \infty\right) \quad \text{(B.1)}$$

Boundary condition at the bottom

$$\frac{\partial \tilde{s}(r,z,p)}{\partial z}\Big|_{z=0} = 0 \quad \text{(B.2)}$$

Boundary condition at the top

$$k_z \frac{\partial \tilde{s}\left(r,z,p\right)}{\partial z}\Big|_{z=b} = -s_y p\tilde{s}\left(r,z,p\right)\Big|_{z=b} \quad \text{(B.3)}$$

Boundary condition at infinity

$$\tilde{s}\left(r,z,p\right)\Big|_{r\to\infty} = 0 \quad \text{(B.4)}$$

Boundary condition at the retaining structure

$$\frac{\partial \tilde{s}\left(r,z,p\right)}{\partial r}\Big|_{r_0\to 0} = \begin{cases} 0 & L < z < b \\ \dfrac{Q}{2\pi r_0 k_r L p} & 0 < z < L \end{cases} \quad \text{(B.5)}$$

Let $\tilde{s}(r,z,p) = F(r,p) \times G(z,p)$, substituting into Eq. (B.1), that is

$$k_r G\frac{\partial^2 F}{\partial r^2} + \frac{k_r G}{r}\frac{\partial F}{\partial r} + k_z F\frac{\partial^2 G}{\partial z^2} = S_s pFG \quad \text{(B.6)}$$

Separating variables for Eq. (B.6), that is

$$\frac{\partial^2 F}{\partial r^2} + \frac{1}{r}\frac{\partial F}{\partial r} - \left(\frac{S_s p + C_m}{k_r}\right)F = 0 \quad \text{(B.7)}$$

$$\frac{\partial^2 G}{\partial z^2} + \frac{C_m}{k_z}G = 0 \quad \text{(B.8)}$$

C_m is the separation constant.

Solve Eq. (B.7) and apply the boundary condition Eq. (B.4), that is

$$F = e_m\left(p\right)K_0\left[\sqrt{\frac{\left(S_s p + C_m\right)}{k_r}}r\right] \quad \text{(B.9)}$$

In Eq. (B.9), $e_m(p)$is a constant. Solve Eq. (B.8) and apply the Eq. (B.2), that is

$$G = f_m\left(p\right)\cos\left(\beta_m z\right) \quad \text{(B.10)}$$

In Eq. (B.10), $\beta_m = \sqrt{C_m/k_z}$,where $f_m(p)$ is a constant. Substituting the Eq. (B.3) into Eq. (B.10), that is

$$\beta_m \sin\left(\sqrt{\beta_m}b\right) = -\frac{s_y}{k_z} p\cos\left(\sqrt{\beta_m}b\right) \quad m = 0,1,2,...,\infty \quad \text{(B.11)}$$

Multiplying Eq. (B.9) and Eq. (B.10), we obtain Eq. (B.12)

$$\tilde{s}(r,z,p)=\sum_{m=0}^{\infty}\lambda_m(p)K_0\left[\sqrt{\frac{S_s p+C_m}{k_r}}r\right]\cos(\beta_m z) \tag{B.12}$$

At this point, $\lambda_{1m}(p)$ is unknown. Solving the Eq. (B.12) using the Eq. (B.5), that is

$$\begin{aligned}\frac{\partial\tilde{s}(r,z,p)}{\partial r}\Big|_{r\to r_0} &= -\sum_{m=0}^{\infty}\lambda_m(p)\sqrt{\frac{S_s p+C_m}{k_r}}K_1\left[\sqrt{\frac{S_s p+C_m}{k_r}}r_0\right]\cos(\beta_m z)\\ &= -\frac{Q}{2\pi r_0 k_r L p} \qquad 0<z<L\\ &= 0 \qquad L<z<b\end{aligned} \tag{B.13}$$

Let $\lambda_m'(p)=\lambda_m(p)\sqrt{S_s p+C_m/k_r}K_1\left[\sqrt{S_s p+C_m/k_r}r_0\right]$, therefore Eq. (B.13) can be expressed as

$$\sum_{m=0}^{\infty}\lambda_m'(p)\cos(\beta_m z)=R(z) \tag{B.14}$$

In the Eq. (B.14)

$$\begin{aligned}R(z) &= 0 \qquad L<z<b\\ &= \frac{Q}{2\pi r_0 k_r L p} \qquad 0<z<L\end{aligned}$$

The left-hand side of Eq. (B.14) is the Fourier series of the function on the right-hand side over the range $0<z<b$. Therefore, the coefficients can be determined using the properties of the Fourier series

$$\begin{aligned}\lambda_m'(p) &= \frac{\int_0^L R(z)\cos(\beta_m z)dz}{\int_0^L \cos^2(\beta_m z)dz}\\ &= \frac{Q\sin(\beta_m L)}{\pi k_r r_0 L p\left[\cos(\beta_m L)\sin(\beta_m L)+\beta_m L\right]}\end{aligned} \tag{B.15}$$

Substituting Eq. (B.15) into Eq. (B.12), obtain the Eq. (17) for the Laplace transform of the drawdown $\tilde{s}$.

Appendix C

C1 water pressure on the right side of the retaining structure

As shown in Fig. 5, and the average hydraulic gradient is $i_m=h-s_w/h-s_w+2D+d$. The seepage force is $j=r_w i_m$. Along the right side of the retaining structure, the water pressure distribution along the streamline $A\to B$ satisfies the following equation

$$-\frac{\partial p_w}{\partial z}-R+\rho_w g=0 \tag{C.1}$$

ρ_w is the density of water, g is the gravitational acceleration. The general solution of Eq. (C.1) is

$$p_w=\rho_w gz-Rz+C \tag{C.2}$$

Combining with the boundary conditions $z=s_w$ and $p_w=0$ on the right side of the retaining structure, that is

$$p_w=\rho_w gz-Rz+C \tag{C.3}$$

Substituting Eq. (C.3) into Eq. (C.2) and then substituting i_m, obtain the Eq. (C.4) for the water pressure, which is also Eq. (21)

$$\begin{aligned}p_{wa} &= \rho_w g(1-i_m)(z-s_w)\\ &= \gamma_w\left(\frac{2D+d}{h-s_w+2D+d}\right)(z-s_w)\end{aligned} \tag{C.4}$$

C2 Water pressure on the left side of the retaining structure

Along the left side of the retaining structure, the water pressure distribution along the streamline $C\to E$ satisfies the following equation

$$-\frac{\partial p_w}{\partial z}+R+\rho_w g=0 \tag{C.5}$$

The general solution of Eq. (C.5) is

$$p_w=\rho_w gz+Rz+C \tag{C.6}$$

Combining with the boundary conditions $y=h$ and $pw=0$ on the left side of the retaining structure, that is

$$C=-Rs_w-\rho_w gs_w \tag{C.7}$$

Substituting Eq. (C.7) into Eq. (C.6) and then substituting i_m, obtain the Eq. (C.8), which is also Eq. (22)

$$\begin{aligned}p_{wp} &= \rho_w g(1+i)(z-h)\\ &= \gamma_w\left(\frac{2(h-s_w+D)+d}{h-s_w+2D+d}\right)(z-h)\end{aligned} \tag{C.8}$$

C3 Earth pressure on the right side of the retaining structure

The soil is subjected to a vertical downward seepage force, this leads to a change in the effective stress of the soil, which alters the active earth pressure acting on the supporting structure. The effective stresses in the water-bearing zone and the non-water-bearing zone are respectively

$$\sigma' = \gamma_s z \qquad z < s_w \tag{C.9}$$

$$\sigma' = \left(\gamma' + j\right) z \qquad z > s_w \tag{C.10}$$

According to Rankine's earth pressure theory, the active earth pressure can be expressed as Eq. (C.11) and Eq. (C.12), which are also Eqs. (23) and (24):

$$p_{sa} = k_a r_s z - 2c\sqrt{k_a} \qquad z < s_w \tag{C.11}$$

$$\begin{aligned} p_{sa} &= k_a\left(\left(\gamma' + j\right)\times z\right) - 2c\sqrt{k_a} \\ &= k_a\left(\left(\gamma' + \gamma_w \frac{h - s_w}{h - s_w + 2D + d}\right)\times z\right) - 2c\sqrt{k_a} \qquad z > s_w \end{aligned} \tag{C.12}$$

C4 Earth pressure on the left side of the retaining structure

The soil is subjected to a vertical upward seepage force, this leads to a change in the effective stress of the soil, which alters the passive earth pressure acting on the supporting structure. The effective stresses in the water-bearing zone and the non-water-bearing zone are respectively

$$\sigma' = \gamma_s z \qquad z < h \tag{C.13}$$

$$\sigma' = \left(\gamma' - j\right) z \qquad z > h \tag{C.14}$$

According to Rankine's earth pressure theory, the passive earth pressure can be expressed as Eq. (C.15) and Eq. (C.16), which are also Eq. (25) and Eq. (26)

$$p_{sp} = k_p \gamma_s z + 2c\sqrt{k_p} \qquad z < h \tag{C.15}$$

$$\begin{aligned} p_{sp} &= k_p\left(\left(\gamma' - j\right) z\right) + 2c\sqrt{k_p} \\ &= k_p\left(\left(\gamma' - \gamma_w \frac{h - s_w}{h - s_w + 2D + d}\right)\times z\right) + 2c\sqrt{k_p} \qquad z > h \end{aligned} \tag{C.16}$$